The Astrophysical Journal, 754:54 (8pp), 2012 July 20 doi:10.1088/0004-637X/754/1/54

EXTREME-ULTRAVIOLET SPECTROSCOPIC OBSERVATION OF DIRECT CORONAL HEATING DURING A C-CLASS SOLAR FLARE

Jeffrey W. Brosius
Catholic University of America at NASA Goddard Space Flight Center, Solar Physics Laboratory, Code 671, Greenbelt, MD 20771, USA; Jeffrey.W.Brosius@nasa.gov
Received 2012 February 10; accepted 2012 May 18; published 2012 July 5

ABSTRACT

With the Coronal Diagnostic Spectrometer operating in rapid cadence (9.8 s) stare mode during a C6.6 flare on the solar disk, we observed a sudden brightening of Fe XIX line emission (formed at temperature $T \approx 8$ MK) above the pre-flare noise without a corresponding brightening of emission from ions formed at lower temperatures, including He I (0.01 MK), O V (0.25 MK), and Si XII (2 MK). The sudden brightening persisted as a plateau of Fe XIX intensity that endured more than 11 minutes. The Fe XIX emission at the rise and during the life of the plateau showed no evidence of significant bulk velocity flows, and hence cannot be attributed to chromospheric evaporation. However, the line width showed a significant broadening at the rise of the plateau, corresponding to nonthermal velocities of at least 89 km s^{-1} due to reconnection outflows or turbulence. During the plateau He I, O V, and Si XII brightened at successively later times starting about 3.5 minutes after Fe XIX, which suggests that these brightenings were produced by thermal conduction from the plasma that produced the Fe XIX line emission; however, we cannot rule out the possibility that they were produced by a weak beam of nonthermal particles. We interpret an observed shortening of the O V wavelength for about 1.5 minutes toward the middle of the plateau to indicate new upward motions driven by the flare, as occurs during gentle chromospheric evaporation; relative to a quiescent interval shortly before the flare, the O V upward velocity was around -10 km s^{-1}.

Key words: Sun: activity – Sun: corona – Sun: flares – Sun: transition region – Sun: UV radiation – Sun: X-rays, gamma rays

1. INTRODUCTION

In the standard model of solar flares (Carmichael 1964; Sturrock 1968; Hirayama 1974; Kopp & Pneuman 1976), energy stored in non-potential coronal magnetic fields is released by reconnection, after which it (1) directly heats the local plasma and (2) accelerates nonthermal particle beams. Thermal conduction and beam particles (and possibly an Alfvén wave Poynting flux, e.g., Fletcher & Hudson 2008, although at present this appears to be observationally indistinguishable from transport by beam particles) can both transport energy to the chromosphere, which will respond with either gentle evaporation or explosive evaporation, depending upon the energy flux (Fisher et al. 1985a, 1985b, 1985c; Brosius & Phillips 2004; Brosius 2009; see also reviews by Antonucci et al. 1999; Bornmann 1999; Fletcher et al. 2011, and references therein). The fractions of released energy that go toward either local heating or nonthermal particle acceleration are not uniform, and may vary from flare to flare depending upon properties like the strength and complexity of the magnetic field as well as the temperature and density of the coronal plasma (which may have been mass loaded or heated by previous nearby flare activity, e.g., Emslie et al. 1992; Brosius 2009). In any case, with spectra and/or images obtained at sufficient cadence to resolve rapid changes (on timescales of tens of seconds) that occur early during a flare's evolution, combined with sufficient temperature resolution to unambiguously distinguish the evolution of "flare" plasma (the ~10 MK plasma that characterizes the very existence of a flare) from the evolution of chromospheric plasma (~0.01 MK), including the heating of chromospheric plasma to transition region (~0.1 MK) and coronal (~1 MK) temperatures, we can gain a better understanding of how the released flare energy is distributed between local heating and particle acceleration (and possibly Alfvén waves), as well as how energy is transported to the chromosphere.

For flares in which most of the energy that is initially released goes toward heating the plasma at the release site to flare temperatures (~10 MK) without accelerating a significant number of particles, chromospheric evaporation is driven by thermal conduction. The EUV signature of this scenario would be the appearance of hot (10 MK) line emission prior to evidence of chromospheric involvement; chromospheric involvement would be observed in the form of velocity flows and brightening of lines formed at temperatures between those of the 10 MK conduction front and the chromosphere (0.01 MK) in which the thermal energy is deposited. For flares in which most of the energy that is initially released goes toward accelerating nonthermal particles (so that direct coronal heating is relatively small, and essentially no 10 MK plasma is produced at the flare's onset), chromospheric evaporation is driven by nonthermal particle beams. The EUV signature of this scenario (e.g., Brosius & Phillips 2004; Brosius & Holman 2009) is the brightening of line emission from ions formed at chromospheric, transition region, and coronal temperatures (created when the beam deposits its energy into the chromosphere and heats it), as well as significant Doppler velocities in those lines, before the appearance of hot, thermal, flare (10 MK) plasma (which is also produced by beam particles heating the chromosphere).

Several previous observations of direct coronal heating have been reported. Brosius & Holman (2007) speculated that the slow but steady rise of weak Fe XIX line emission early during their observations of a flarelike transient with the Coronal Diagnostic Spectrometer (CDS; Harrison et al. 1995) aboard the *Solar and Heliospheric Observatory* (*SOHO*) spacecraft and the *Ramaty High Energy Solar Spectroscopic Imager* (*RHESSI*; Lin et al. 2002; Hurford et al. 2002; Smith et al. 2002) satellite may have been due to direct coronal heating. This was based on the fact that emission lines formed at lower temperatures showed no simultaneous intensity enhancements, indicating that

the chromosphere was not involved in the event at those times. Brosius (2009) presented further evidence for direct coronal heating based on EUV spectra obtained during an M1.5 flare, but argued that the observations were not conclusive due in large part to the rapid and extensive fluctuations in the light curves. Su et al. (2009) found that X-ray brightenings observed with both *RHESSI* and the X-Ray Telescope (XRT; Golub et al. 2007) aboard *Hinode* during a C8.5 flare appeared about 20 minutes earlier than the EUV brightenings seen in *Transition Region And Coronal Explorer* (*TRACE*; Handy et al. 1999) 171 Å images and filament activations seen in Hα images from the Mauna Loa Solar Observatory. They interpreted this as an indication that the X-ray emission may have been caused by direct coronal heating due to reconnection, but the energy transported down to the chromosphere was insufficient to produce simultaneous EUV brightenings.

Several studies have related early enhancements in the soft X-ray nonthermal line widths to flare energy release. For example, Alexander et al. (1998) found that the nonthermal width of soft X-ray emission lines observed with the Bragg Crystal Spectrometer (BCS; Culhane et al. 1991) aboard the *Yohkoh* satellite either exhibited a maximum prior to the first significant burst of hard X-rays observed with *Yohkoh*'s Hard X-ray Telescope (HXT; Kosugi et al. 1991), or was already decaying from an earlier unobserved maximum at the time of the first significant burst of hard X-rays. They interpreted the nonthermal broadening as a direct result of the flare energy release process rather than a consequence of that energy's deposition. Their Figures 1 and 2 show nonthermal velocities between 60 and 200 km s^{-1}. Harra et al. (2001) observed two flares with BCS and HXT during one *Yohkoh* orbit, and found that the soft X-ray line widths diminished to the active region (non-flaring) level between the flares, and then began to rise above this background level 11 minutes before the start of the second flare as defined by the start of the hard X-ray emission. While the nonthermal width increased, there was no increase in the light curves or the electron temperature, leading them to suggest that observed turbulent changes were related to the flare trigger mechanism. Nonthermal velocities between about 50 and 250 km s^{-1} were observed.

In this work, we present EUV spectroscopic evidence for direct coronal heating during a C6.6 flare observed by CDS on 2011 February 15. In Section 2, we present our observations and results, and in Section 3 we discuss and summarize our conclusions.

2. OBSERVATIONS AND RESULTS

We observed AR 11158 (S20W21) for more than eleven hours (11:52–22:55 UT) with CDS on 2011 February 15. CDS ran the FLAREDOP study, which provides rapid cadence (9.8 s) stare spectra within each of the twelve $4'' \times 20''$ segments into which its $4'' \times 240''$ slit was divided. Spectra include emission lines of ions formed in the upper chromosphere (He I, at temperature $T \approx 0.01$ MK), the transition region (O V, $T \approx 0.25$ MK), the corona (Si XII, $T \approx 2$ MK), and only during flares (Fe XIX, $T \approx 8$ MK). These were calibrated and analyzed with standard SolarSoftWare IDL procedures. We fit broadened Gaussian profiles (Thompson 1999; see also Brosius 2003; Brosius & Phillips 2004) to emission lines of He I at 522.2 and 584.3 Å, O V at 629.7 Å, Si XII at 520.7 Å, and Fe XIX at 592.2 Å in each of the twelve slit segments for all 4060 exposures obtained during the observing run. The Fe XIX line at 592.2 Å is present in CDS spectra only associated with flares, so for times outside of flares we simply applied the Fe XIX line profile fit structure to the noise around 592 Å to obtain a measure of the background noise on the line's integrated intensity. (For a given line profile fit structure in IDL, one can always derive an amplitude, centroid wavelength, and width even if no line, but only noise, is present.) For completeness, and to help obtain the most reliable measure of the background noise around the Fe XIX wavelength, we included in our fitting procedure the weak Fe XII line at 592.6 Å first identified by Del Zanna & Mason (2005) in off-limb spectra above quiet areas. The He I line at 584.3 Å became saturated for an extended period during our observing run, so we do not use it in what follows. Here, we focus on the sudden, rapid brightening of Fe XIX emission, which occurred without corresponding brightenings in the lines formed at lower temperatures, seen by CDS around 19:47 UT during a *GOES* C6.6 flare that started around 19:30 UT. We attribute the Fe XIX brightening to direct coronal heating.

We used the *Solar Dynamics Observatory* (*SDO*) Atmospheric Imaging Assembly (AIA; Lemen et al. 2012; Boerner et al. 2012) Cutout Service to acquire images of AR 11158 in AIA's seven EUV channels (94, 131, 171, 193, 211, 304, and 335 Å) from 19:00 to 21:00 UT. Movies in all of these channels show that the flare started around 19:30 UT about an arcmin west of the CDS slit. Three images from each of the 304 and 94 Å channels are shown in Figure 1, where frames (a) and (b) show images obtained late during the quiescent period before the flare started, frames (c) and (d) show images obtained nearly 6 minutes after the start of the C6.6 flare, and frames (e) and (f) show images obtained shortly after the end of an ill-timed AIA calibration run (19:45–20:05 UT), by which time the flare is clearly seen in both channels at the location of the CDS slit (particularly in the 7th $4'' \times 20''$ segment up from the bottom, indicated with an arrow in Figure 1(b)). The twelve $4'' \times 20''$ segments into which the CDS slit spectra were separated are overplotted in each frame of Figure 1. Hereafter we refer to individual such segments simply as the *n*th slit segment, starting from 1 and counting up from the bottom. The slit's pointing was held fixed at (+304.″6, −254.″0). In the continuing, extended phase of the *SOHO* mission the spacecraft's roll angle is oriented such that ecliptic north is at the top of the CDS slit, which for the present observations means that the slit was rotated −2.°40 relative to solar north. The unfortunate AIA calibration run included a focus sweep starting at 19:45 UT, a filter wheel filter check starting at 19:55 UT, and a front filter check starting at 20:00 UT. Thus, AIA missed the sudden, rapid brightening of Fe XIX emission observed by CDS around 19:47 UT that is key to the present investigation. We also checked for coordinated observations with *RHESSI*, but found that while it observed the beginning and the end of the C6.6 flare, it entered the South Atlantic Anomaly around 19:38 UT and night around 20:02 UT, and so also missed the Fe XIX brightening observed by CDS.

Figure 2 shows light curves and relative Doppler velocities for Fe XIX and O V obtained in the 7th slit segment (see Figure 1) over an 8 hr period during our observing run. We refer here and in what follows to "relative Doppler velocities" because CDS, like most solar UV and EUV spectrometers, provides no absolute wavelength scale; this is discussed in greater detail below. Two features seen in Figure 2 enlighten our analysis of direct coronal heating during the C6.6 flare. First, because Fe XIX is absent from CDS spectra that are not associated with flares, we need EUV spectra from flares like those in Figure 2(a) in order to derive the Fe XIX "reference wavelength" against which to measure relative Doppler velocities. Second is the long-duration

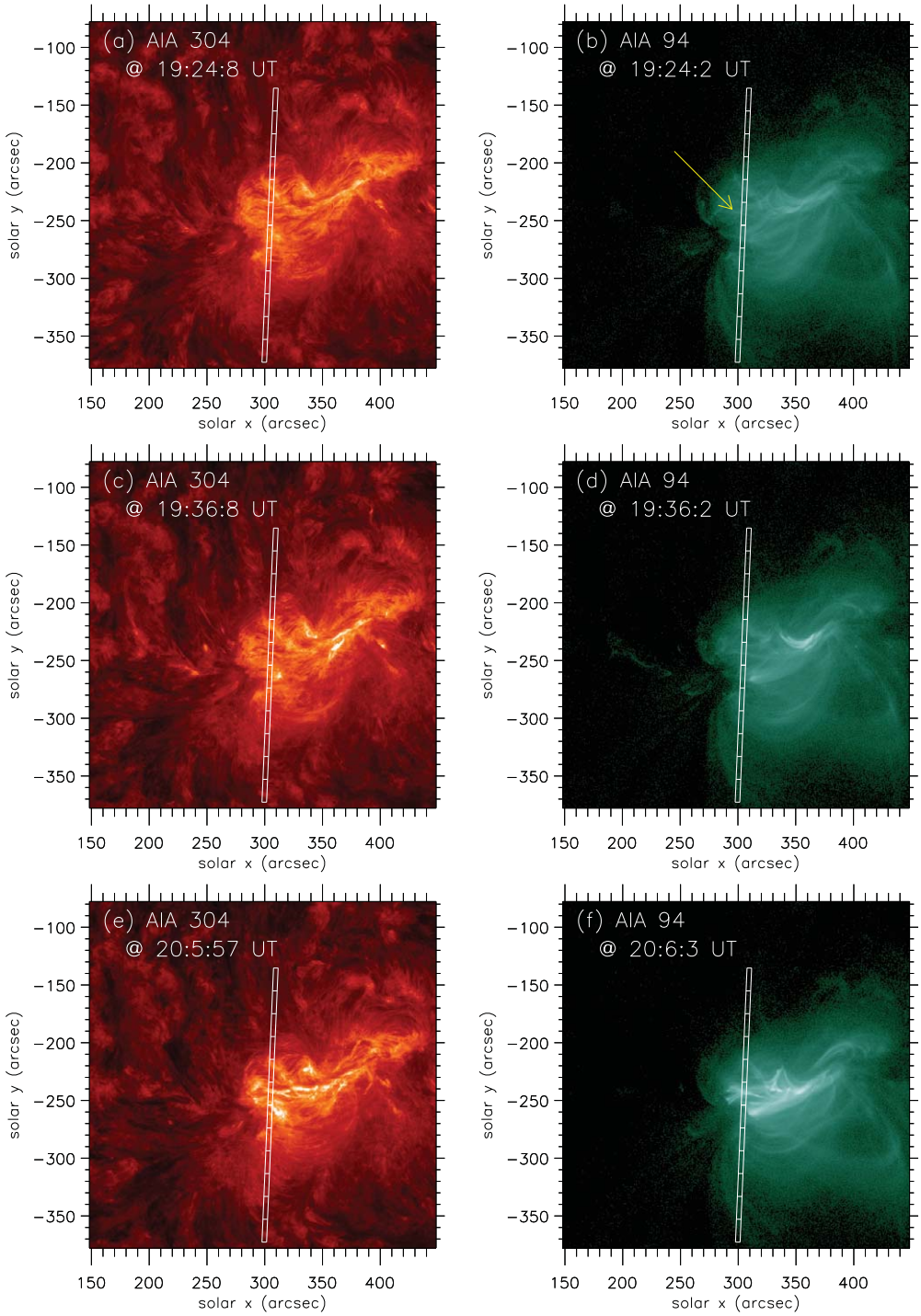

Figure 1. Images from AIA's 304 Å (left column) and 94 Å (right column) channels at selected times around the C6.6 flare on 2011 February 15. The twelve $4'' \times 20''$ segments into which CDS slit spectra were averaged are overplotted, and show the $-2.^{\circ}40$ tilt of the slit relative to solar north. The top row (frames (a) and (b)) shows images obtained late during the quiescent period before the flare started at 19:30 UT; the middle row (frames (c) and (d)) shows images obtained nearly 6 minutes after the start of the *GOES* flare; the bottom row (frames (e) and (f)) shows images obtained shortly after the end of the ill-timed AIA calibration run (19:45–20:05 UT), by which time flare brightening is evident at the location of the CDS slit (particularly the 7th segment, indicated with an arrow in frame (b)).

apparent redshift in O v emission, which we need to be aware of when examining the O v velocities close to the C6.6 flare.

The C6.6 flare first became evident at the location of the CDS slit with a rapid increase of Fe xix emission to a relatively constant level, or plateau, in the light curve obtained in the 7th slit segment. No similar rise in Fe xix emission was observed in any of the other slit segments. See Figure 3, in which normalized CDS light curves over the lifetime of the C6.6 flare help to put the Fe xix plateau in perspective. We define the start of the plateau, and hence the effective start of the flare at the location of the CDS slit, as the time at which the Fe xix intensity exceeded and remained greater than 1σ above its average noise level derived from the quiescent interval 19:33:06–19:46:37 UT (a fairly flat minimum of EUV emission between the C1.7 and C6.6 flares; see Figure 4(a) and Table 1); this occurred at 19:47:26 UT. A similar approach for He i, O v, and Si xii reveals that they

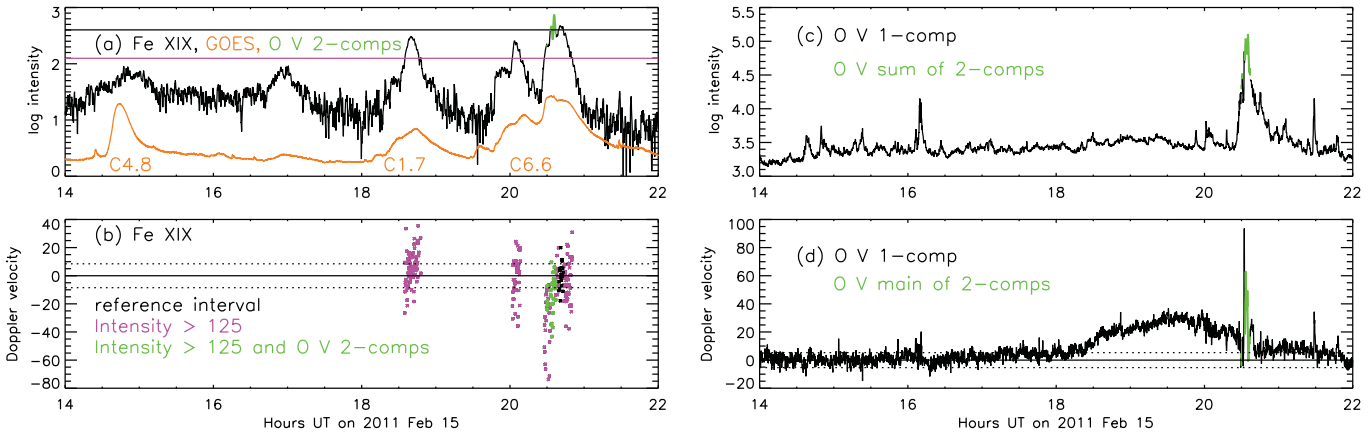

Figure 2. (a) Log of integrated Fe XIX line intensity (erg cm^{-2} s^{-1} sr^{-1}), smoothed with a five-point running boxcar, in the 7th slit segment (see Figure 1). Exposures with intensities greater than 400 erg cm^{-2} s^{-1} sr^{-1} (indicated with a black horizontal line), obtained after the intervals in which O V exhibited a significant secondary blueshifted component (20:30:00–20:30:28 UT and 20:32:44–20:37:00 UT) were used to derive the Fe XIX reference wavelength and its associated 1σ scatter (8.5 km s^{-1}; dotted horizontal lines in frame (b)). The *GOES* 1–8 Å light curve, displayed on an arbitrary logarithmic scale to fit in this figure, is overplotted and labeled with flare category. (b) Relative Doppler velocity (km s^{-1}) in the exposures used to derive the "reference wavelength" (black), in the exposures in which O V exhibited a significant, secondary blueshifted component (green), and in the exposures in which the Fe XIX intensity exceeds 125 erg cm^{-2} s^{-1} sr^{-1}. The solid horizontal line indicates zero relative velocity, and the dashed horizontal lines indicate $\pm1\sigma = \pm8.5$ km s^{-1}. Negative velocities correspond to blueshifted emission, and positive to redshifted. (c) Log of integrated O V line intensity (erg cm^{-2} s^{-1} sr^{-1}) in the 7th slit segment. When a secondary blueshifted component is observed, the displayed intensity is the sum of the intensities of the two components. (d) Relative Doppler velocity based on a "reference wavelength" averaged over the first 2001 exposures of the sequence (11:52:20–17:18:39 UT). When a secondary blueshifted component is observed, the displayed velocity is for the main component only. The solid horizontal line indicates zero relative velocity; dashed horizontal lines indicate $\pm1\sigma = \pm5.3$ km s^{-1}.

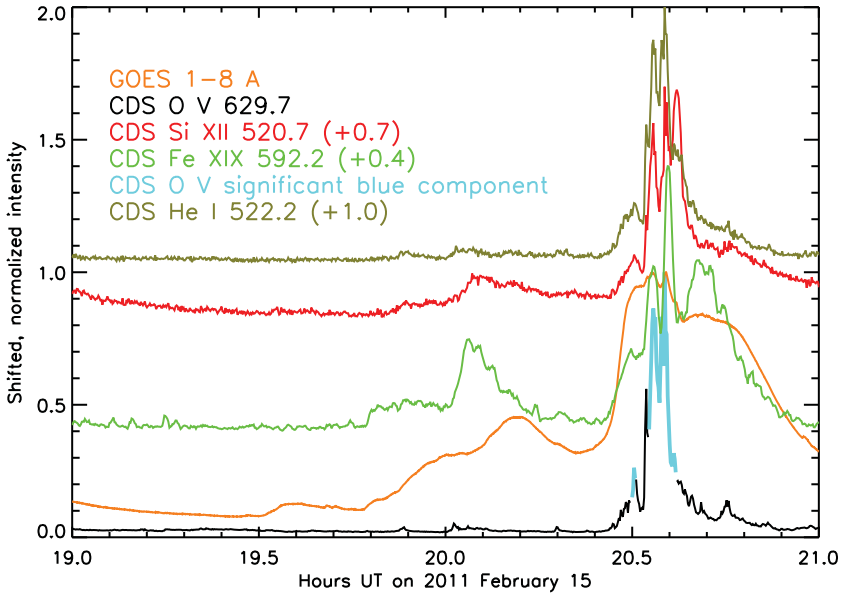

Figure 3. Normalized, offset (by amounts indicated in the figure legend) light curves for a 2 hr period in the 7th slit segment. Fe XIX is smoothed with a five-point running boxcar. Although *GOES* light curves and AIA images indicate that the flare started around 19:30 UT, the event did not begin at the location of the CDS slit until the sudden brightening to a plateau of Fe XIX emission around 19:47 UT.

brightened several minutes after Fe XIX, starting at 19:51:03, 19:52:11, and 19:52:30 UT, i.e., at progressively later times with increasing line formation temperature. This tells us that the emergence of the plateau of Fe XIX emission cannot be due to chromospheric evaporation driven by nonthermal particle beams (or Alfvén waves), because if that were the case then the emission of the lower temperature lines would have brightened earlier than (or, at the latest, in the case of a very large energy flux, simultaneously with) the Fe XIX emission. Figure 4(b) shows O V light curves in the two slit segments directly above and the two slit segments directly below the 7th. These and the O V light curve of Figure 4(a) reveal that no impulsive O V brightening occurred within a 100″ length of the slit prior to the Fe XIX plateau. This provides further confirmation, within the limited field of view of the fixed slit position, that the Fe XIX plateau is not produced by chromospheric evaporation driven by nonthermal particles. The brightening of He I, O V, and Si XII at progressively later times with increasing temperature during the Fe XIX plateau could be due to thermal conduction from the heated Fe XIX source, or to a weak beam of nonthermal particles (or weak Poynting flux of Alfvén waves) that commenced during the plateau.

Because CDS provides no absolute wavelength scale, we measure Doppler shifts for specific events (like flares or flare precursors) relative to "reference wavelengths" obtained by averaging the centroid values derived for individual emission

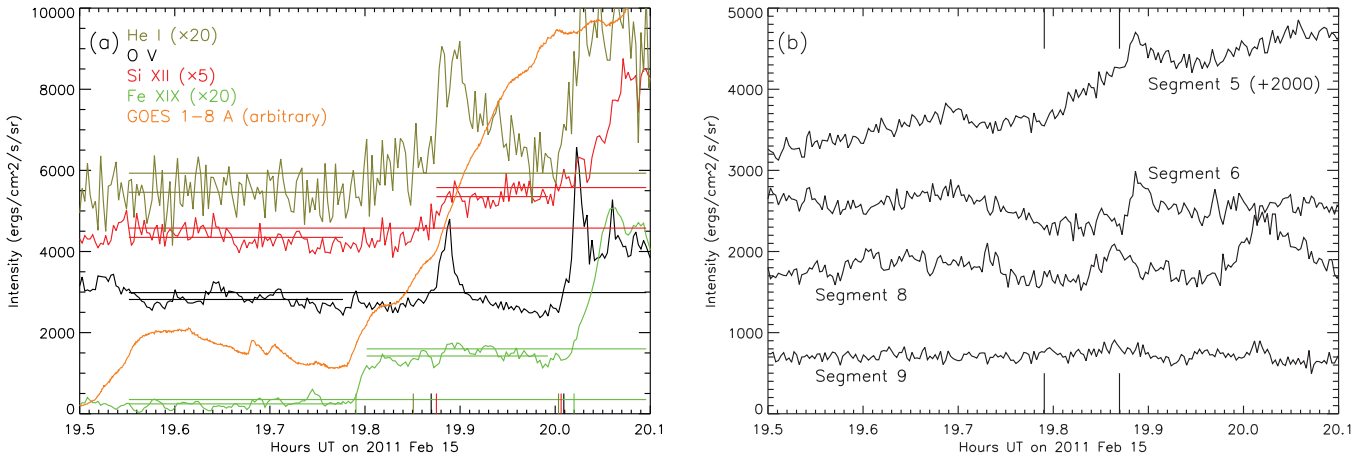

Figure 4. (a) CDS light curves of four lines in the 7th slit segment around the time that the flare starts at the position of the CDS slit. The O v line is displayed on an absolute intensity scale, and the other line intensities are scaled (as indicated in upper left) for ease of comparison. The Fe XIX intensity was smoothed with a five-point running boxcar, and the *GOES* 1–8 Å curve is displayed on an arbitrary scale. Short, color-coded horizontal lines indicate average intensities of the corresponding emission lines within the quiescent interval 19:33:06–19:46:37 UT; the length of the horizontal lines corresponds to this interval. The long, color-coded horizontal lines indicate 1σ above the average intensities, and are used to determine the times at which line intensities continuously exceed their pre-event quiescent values by more than 1σ. Color-coded extra-long vertical tick marks indicate times at which the lines do this. The Fe XIX intensity starts a rapid increase to its plateau at 19:47:26 UT. The additional green horizontal lines correspond to average intensity in the Fe XIX plateau and 1σ above this average intensity. These and a similar pair of red horizontal lines in the Si XII plateau are used to determine the time of the post-plateau brightenings. Times and intensities indicated in this figure are listed in Table 1. (b) CDS O v light curves in the two slit segments directly above the 7th, and the two directly below, as labeled. Note that no impulsive brightening is observed prior to the Fe XIX plateau (indicated by the first extra-long vertical tick mark, at 19:47:26 UT) in any of these O v light curves. The second extra-long vertical tick mark indicates the rise in O v emission in the 7th segment (19:52:11 UT).

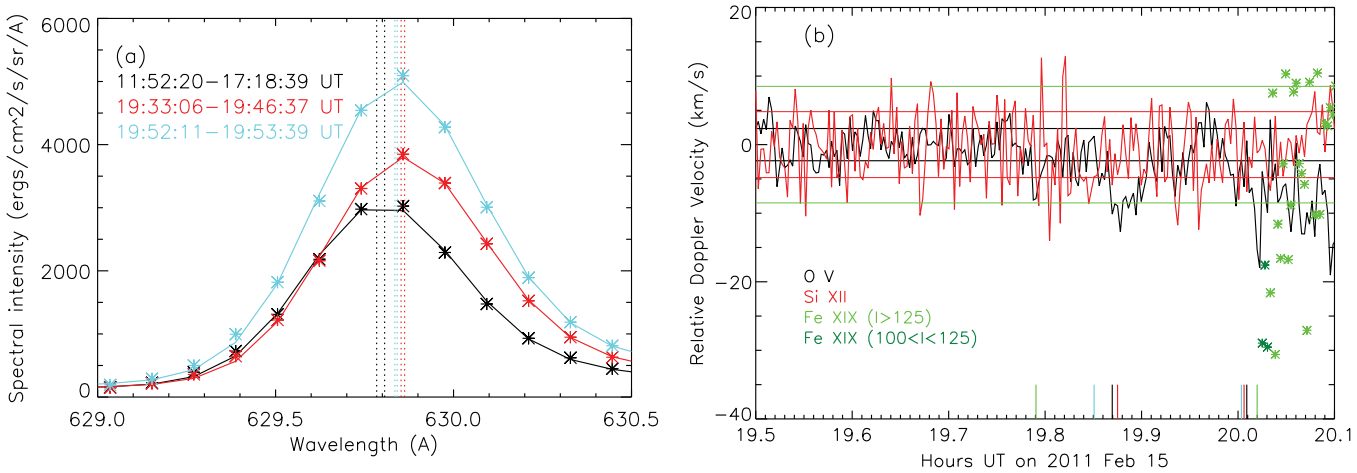

Figure 5. (a) Profiles of the O v 629.7 Å emission line observed by CDS in the 7th slit segment, averaged over the first 2001 exposures of the observing run (11:52:20–17:18:39 UT, black symbols and curve), the pre-flare quiescent interval (19:33:06–19:46:37 UT, shown in red), and toward the middle of the Fe XIX plateau (19:52:11–19:53:39 UT, blue). Color-coded vertical dashed lines indicate $\pm 1\sigma$ from the associated centroid wavelengths, which correspond to uncertainties of ± 5.3, ± 2.3, and ± 1.6 km s^{-1} on the relative Doppler velocities. Although both of the later intervals appear redshifted relative to the earliest, the O v profile averaged over the middle of the Fe XIX plateau is blueshifted about -9.0 km s^{-1} relative to the O v profile averaged over the quiescent interval. (b) Relative Doppler velocities from lines observed with CDS, where solid, color-coded horizontal lines indicate 1σ scatter on O v (2.3 km s^{-1}, black), Si XII (4.8 km s^{-1}, red), and Fe XIX (8.5 km s^{-1}, green). Reference wavelengths and uncertainties for O v and Si XII here are from the quiescent interval shortly before the Fe XIX plateau (19:33:06–19:46:37 UT), when the O v emission was redshifted relative to the first 2001 exposures in the series. Note the significant upward (negative) velocity in O v during the Fe XIX plateau, indicating gentle chromospheric evaporation. Light green asterisks correspond to velocities in exposures with Fe XIX intensity greater than 125, and the (three) darker green asterisks are for $100 \leqslant I \leqslant 125$. Note that Fe XIX, like O v, is blueshifted to start the post-plateau brightening.

line profile fits over comparatively quiescent intervals. For example, the O v reference wavelength against which the relative Doppler velocities in Figure 2(d) were derived was obtained by averaging the centroid values of the line profile fits in the first 2001 exposures (11:52:20–17:18:39 UT) for the 7th slit segment. The uncertainty on the wavelength is derived from the scatter in the centroid measurements within the same exposures, which for O v corresponds to a velocity uncertainty of 5.3 km s^{-1}. In the case of O v, note the long-term trend in which the relative Doppler velocity increased (became redshifted, directed downward) around 18:15 UT, reached a maximum of about +35 km s^{-1} near 19:30 UT, and by about 21:30 UT declined to a value not significantly different from zero. This trend is not instrumental in origin because the same shift is not observed in the other slit segments, nor is it observed uniformly in the other lines. It is, therefore, solar in origin, possibly due to intrinsic differences in the solar features that move with solar rotation across the fixed pointing of the slit, or

Table 1
EUV Line Emission During CDS Observation of Direct Coronal Heating

Line	log T (K)	I_{quiet} [a]	t_{start} [b]	$I_{plateau}$ [c]	$t_{post\text{-}plateau}$ [d]
Fe XIX 592.2 Å	6.89	12.1 ± 5.6	19:47:26	71.0 ± 9.4	20:01:11
Si XII 520.7 Å	6.27	869.6 ± 45.6	19:52:30	$1071. \pm 44.$	20:00:23
O V 629.7 Å	5.37	$2817. \pm 170.$	19:52:11	...	20:00:33
He I 522.2 Å	4.	273.0 ± 23.5	19:51:03	...	20:00:13

Notes.
[a] Pre-event quiescent intensity in erg cm^{-2} s^{-1} sr^{-1}, averaged over the time interval 19:33:06–19:46:37 UT. For Fe XIX, this corresponds to noise (and its scatter).
[b] Time (UT) after which the line intensity continuously exceeds I_{quiet}.
[c] Plateau intensity in erg cm^{-2} s^{-1} sr^{-1}, averaged over the time interval 19:48:06–19:59:33 UT for Fe XIX and 19:52:41–19:59:33 UT for Si XII. For O V and He I, continue to use the pre-event average quiescent intensity.
[d] Time (UT) after which the Fe XIX and Si XII line intensities continuously exceed their respective average plateau values $I_{plateau}$, and the O V and He I line intensities again exceed their respective average pre-event values I_{quiet}.

perhaps due to downflowing material ("warm rain") that had been heated and evaporated upward during the earlier C1.7 flare. (Si XII, not shown here, reveals a shorter-duration, smaller-velocity version of this behavior.)

Whatever the origin of the long-duration redshift in O V emission, our interest here in wavelength *shifts* (as opposed to absolute wavelength measurements) observed in rapid cadence flare stare spectra means that our choice of reference interval is primarily one of convenience, and does not necessarily correspond to one of absolute rest. For the sake of consistency with the light curve analysis described above, we use the same quiescent interval (19:33:06–19:46:37 UT, see Figure 4(a) and Table 1) that was used to determine the flare start times to derive reference wavelengths and their associated uncertainties for He I, O V, and Si XII. See Figure 5(a), which shows O V line profiles averaged over the first 2001 exposures of the observing run, over the pre-flare quiescent interval (when the O V profile was redshifted about 29.5 km s^{-1} relative to the first 2001 exposures in the series), and over a portion of the Fe XIX plateau (19:52:11–19:53:39 UT) in which the O V wavelength became significantly shorter than the wavelength in the pre-flare quiescent interval. Shifts among these three profiles are evident. Although the O V profile during the Fe XIX plateau is redshifted about 20.5 km s^{-1} relative to the first 2001 exposures of the observing run, this redshift was less than the redshift of about 29.5 km s^{-1} (again relative to the first 2001 exposures of the observing run) during the quiescent interval immediately preceding the Fe XIX plateau. Thus, the O V profile for about 1.5 minutes (19:52:11–19:53:39 UT) during the plateau is blueshifted (-9.0 km s^{-1}) relative to the quiescent interval. See Figure 5(b), in which the O V and Si XII Doppler velocities are calculated relative to the quiescent interval (19:33:06–19:46:37 UT). We interpret the decrease observed in the O V wavelength during the plateau to indicate new upward motions driven by the flare, as occurs during gentle chromospheric evaporation. Note, though, that Si XII shows no significant relative velocities at the same times. Our interpretation is muddied by the fact that the Fe XIX plateau itself occurs during the period of long-duration O V redshift relative to the first 2001 exposures in our sequence. Assuming that the long-duration O V redshift is due to warm rain, and considering the hydrodynamic simulations of Emslie et al. (1992; see also Brosius 2009) in which upward velocities are reduced by the increased inertia of the overlying material, we speculate that the decrease in O V redshift by about 9 km s^{-1} during the plateau indicates a reduction in downward momentum of the warm rain by gently evaporated material that is attempting to flow upward. Keeping in mind that neither the first 2001 exposures of our observing sequence nor our quiescent reference interval shortly before the flare correspond to absolute rest frames, we recognize that alternative explanations may be viable.

Allowing for the possibility of secondary, highly blueshifted components as reported for M-class flares by Brosius (2003) and Veronig et al. (2010), and for B-class flares as reported by Brosius & Holman (2010) and Chen & Ding (2010), we fit the lines of Si XII 520.7 Å, He I 522.2 Å, and O V 629.7 Å with two broadened Gaussian components: a "main" component whose centroid was confined to about ±0.3 Å of the line's nominal rest wavelength and a "secondary" component whose centroid was confined to values shortward of the main component's range. See Brosius & Holman (2010) for a description of how the significance of the secondary component is quantified. For all three lines, we find a secondary, highly blueshifted ($v < -200$ km s^{-1}, i.e., upward velocities in excess of 200 km s^{-1}) component in several time intervals. It lasted the longest for O V, where it occurred from 20:30:00 to 20:30:28 UT, and from 20:32:44 to 20:37:00 UT. Only for O V did the secondary component's intensity briefly rival that of the main component. We mention the secondary, blueshifted component mainly because we deliberately exclude exposures with significant such emission from those over which we obtain the Fe XIX reference wavelength (and width) and its associated 1σ scatter. In other words, we avoid intervals that are clearly turbulent when calculating the Fe XIX reference quantities. We found that no significant, secondary, blueshifted components were observed during the incident of direct coronal heating under investigation in the present work, nor did the Fe XIX line show such a component at any time during these observations. As an aside we mention that the present work, combined with the above references, indicates that prominent, highly blueshifted, secondary components to the O V emission line at 629.7 Å have now been observed in B-, C-, and M-class flares.

Fe XIX emission is present in CDS spectra only associated with flares, so we cannot establish a "reference wavelength" for it like we can for the other lines based on quiescent intervals. Instead, we consider the Fe XIX line to be at rest when its intensity approaches its largest value during a flare under the assumption that this occurs when flare loops are filled with hot emitting plasma, and bulk motions have mostly ceased. To obtain an Fe XIX reference wavelength and its associated uncertainty, we use CDS exposures in which the Fe XIX intensity exceeds 400 erg cm^{-2} s^{-1} sr^{-1} (note the horizontal black line in Figure 2(a)), but exclude those in which He I, O V, and Si XII exhibit highly blueshifted secondary components (note the green-colored portion of the Fe XIX light curve in Figure 2(a)). Velocities derived for these individual exposures are displayed as black asterisks (clustered near 0 km s^{-1}) in Figure 2(b). We subsequently derived relative Doppler velocities for exposures in which the intensity exceeds 125 erg cm^{-2} s^{-1} sr^{-1} (including those with multiple O V components), also shown in Figure 2(b). This figure shows that the Fe XIX emission is mainly at rest during the three flare peaks in our observation, but that significant blueshifts occurred early during the main phase of the C6.6 flare (corresponding to upward velocities approaching -80 km s^{-1}), as well as during the multi-component interval (-40 km s^{-1}).

The blueshifts are consistent with chromospheric evaporation during the main phase of the flare.

The Fe XIX profiles during the rapid emergence of the plateau as well as during the plateau itself are too weak and noisy to obtain reliable relative Doppler velocity measurements in the individual exposures. To look for evidence of velocity flows at those times, we averaged the line profiles during an 11-exposure interval covering the plateau's emergence (19:47:16–19:48:57 UT) and during the entire plateau (19:48:06–19:59:33 UT), and found that neither of those profile fits yielded a wavelength significantly different from the reference value. Thus, the Fe XIX emission during the rise and life of the plateau reveals no evidence of significant velocity flows, and hence cannot be attributed to chromospheric evaporation (driven by any mechanism).

We also derived Fe XIX's "reference width" and its associated uncertainty ($W_{\rm ref} = 0.5908 \pm 0.0431$ Å) from the same CDS exposures used to derive the reference wavelength. This width includes contributions due to instrumental broadening (which dominates the width; see Harrison et al. 2002), thermal broadening, and unresolved turbulent motions. Based on the same averaged profiles described above for the plateau's emergence and the plateau's duration, we find a significant broadening only during the emergence ($W_{\rm emerg} = 0.6588$ Å). Knowing that the instrumental broadening is the same for both $W_{\rm ref}$ and $W_{\rm emerg}$, and assuming that the thermal broadening is the same for both, we derive a lower limit on the nonthermal velocity at the start of the plateau $V_{\rm nonth} = c(W^2_{\rm emerg} - W^2_{\rm ref})^{1/2}/(\lambda_{\rm ref}(4\ln(2))^{1/2}) = 89$ km s^{-1}, where $\lambda_{\rm ref}$ is the reference wavelength. We refer to this as a lower limit because we did not remove whatever turbulent component may be present in $W_{\rm ref}$, and so removed some turbulent contribution from $W_{\rm emerg}$ when calculating $V_{\rm nonth}$. We can compensate for this by incorporating the nonthermal turbulent velocity in the background active region found by Harra et al. (2001; 34 km s^{-1} in S XV and 66 km s^{-1} in Ca XIX) to obtain a total turbulent velocity between 95 and 111 km s^{-1}. Even without the added background turbulence, this is consistent with the nonthermal velocity of about 100 km s^{-1} measured by Hara et al. (2011) in lines of Fe XXIII and Fe XXIV observed in raster mode with the Extreme-ultraviolet Imaging Spectrometer (EIS; Culhane et al. 2007) aboard *Hinode* during the impulsive phase of a B9.5 flare.

After the plateau of Fe XIX emission, the intensities of He I, O V, Si XII, and Fe XIX were all seen to brighten rapidly to values greater than their maxima during the plateau. Because the He I and O V intensities decreased during the plateau back to their pre-flare quiescent values, we used the pre-flare average quiescent intensities and their associated uncertainties (see Table 1 and Figure 4(a)) to determine post-plateau brightening start times of 20:00:13 and 20:00:33 UT, respectively. Because the Fe XIX and, to a lesser extent, Si XII intensities remained fairly constant during the plateau (see Figure 4(a)), we used plateau-averaged intensities for these lines to determine post-plateau start times of 20:01:11 and 20:00:23 UT. Thus, He I, O V, and Si XII all started 48 ± 10 s earlier than Fe XIX (i.e., simultaneously within the 9.8 s cadence of the observations), which suggests that the post-plateau brightening is driven by nonthermal beams. Figure 5(b), in which the O V and Si XII Doppler velocities are calculated relative to the quiescent pre-flare interval (19:33:06–19:46:37 UT), shows that both O V and Fe XIX (but not Si XII) were blueshifted at this time (note especially the dark green asterisks that correspond to CDS exposures for which the Fe XIX intensity exceeded 100 but was less than 125 erg cm^{-2} s^{-1} sr^{-1}), consistent with gentle chromospheric evaporation (Fisher et al. 1985a, 1985b, 1985c; Brosius & Phillips 2004; Brosius 2009).

3. DISCUSSION AND SUMMARY

We summarize the results of our rapid cadence (9.8 s) EUV spectroscopic observation of a C6.6 flare: (1) the Fe XIX intensity increased rapidly to a plateau at 19:47:26 UT, after which it exceeded its pre-flare noise level by more than 1σ (by a factor ∼6); (2) during the plateau He I, O V, and Si XII, formed at progressively greater temperatures of 0.01, 0.25, and 2.0 MK, respectively, brightened at progressively later times of 19:51:03, 19:52:11, and 19:52:30 UT; (3) O V showed a Doppler blueshift (relative to the average wavelength measured in the quiescent interval 19:33:06–19:46:37 UT shortly before the plateau) interpreted as an upward velocity around −10 km s^{-1} from 19:52:11 to 19:53:39 UT during the plateau, suggesting gentle chromospheric evaporation; (4) the Fe XIX profiles in the individual exposures obtained before and during the plateau are too weak and noisy to measure significant changes in centroid wavelength or width, but the profile averaged over the lifetime of the plateau reveals no significant changes in wavelength or width relative to the corresponding "reference" values, and the profile averaged over the early rise of the plateau (19:47:16–19:48:57 UT) reveals a significant increase in line width that corresponds to an increase in turbulent velocity of 89 km s^{-1}, but no change in centroid wavelength; and (5) the post-plateau brightening exhibited behavior consistent with gentle chromospheric evaporation.

Based on the behavior of the intensities, relative Doppler velocities, and nonthermal broadening observed with CDS, the most likely explanation for the plateau of Fe XIX emission is direct heating by magnetic reconnection in the coronal plasma. Alternative explanations for the observed plateau of Fe XIX emission include (1) heated plasma from the flare's 19:30 UT starting position west of the slit moving into the location of the slit, and falling down along field lines after having been evaporated upward during chromospheric evaporation, or (2) thermal conduction from a hot source outside the CDS field of view (again, perhaps, from the flare's starting position farther to the west). Although these two possibilities cannot be ruled out completely, the first appears to be unlikely in light of the absence of redshifts associated with the emergence of the plateau (i.e., nothing appears to be falling down from elsewhere), and the second appears to be less likely than the direct heating (by reconnection) scenario in light of the Fe XIX line broadening at the onset of the plateau.

It is worth mentioning that we see a short-lived (one exposure) O V enhancement that barely exceeds the pre-flare average intensity by 1σ at the start of the Fe XIX plateau (see Figure 4(a)). The Doppler velocity (relative to the quiescent interval shortly before the flare) also shows a short-lived (three exposures) significant upflow with a maximum velocity around −8 km s^{-1} at the same time. This suggests the possibility that a very weak beam drove short-lived gentle chromospheric evaporation at the onset of the Fe XIX plateau, but failed to raise the chromosphere's temperature to 2 MK or greater because no simultaneous increase in the Si XII intensity was observed.

The AIA calibration run from 19:45 to 20:05 UT is extremely unfortunate, as our relatively rare spectroscopic observation of direct coronal heating would have provided an opportunity to verify or suggest improvements to Brosius & Holman's (2012) method of using AIA to determine whether flare energy transport

is dominated by thermal conduction or by nonthermal particles (the latter of which at present appears to be indistinguishable from transport by a Poynting flux of Alfvén waves, as described by Fletcher & Hudson 2008). Briefly, the method relies on the fact that the temperature response functions (Boerner et al. 2012) of all of the AIA EUV channels are sensitive to emission from plasma in the 0.1–0.7 MK temperature range, and so all would simultaneously detect chromospheric heating to such temperatures in the case of beam energy transport. If transport is by conduction, only the channels sensitive to higher, "flare" temperatures (∼10 MK; 94, 131, 193, 335 Å) would detect such heated plasma first, followed by those that are insensitive to such high temperatures (171, 211 Å) while the chromosphere is heated (by thermal conduction) through temperatures to which they are sensitive. Future spectroscopic stare observations with CDS and EIS at cadences comparable to those of AIA (12 s) will help to verify this technique.

J.W.B. acknowledges NASA support through SR&T grant NNX10AC08G.

REFERENCES

Alexander, D., Harra-Murnion, L. K., Khan, J. I., & Matthews, S. A. 1998, ApJ, 494, L235
Antonucci, E., Alexander, D., Culhane, J. L., et al. 1999, in The Many Faces of the Sun, ed. K. T. Strong, J. L. R. Saba, B. M. Haisch, & J. T. Schmelz (New York: Springer), 331
Boerner, P., Edwards, C., Lemen, J., et al. 2012, Sol. Phys., 275, 41
Bornmann, P. L. 1999, in The Many Faces of the Sun, ed. K. T. Strong, J. L. R. Saba, B. M. Haisch, & J. T. Schmelz (New York: Springer), 301
Brosius, J. W. 2003, ApJ, 586, 1417
Brosius, J. W. 2009, ApJ, 701, 1209
Brosius, J. W., & Holman, G. D. 2007, ApJ, 659, L73
Brosius, J. W., & Holman, G. D. 2009, ApJ, 692, 492
Brosius, J. W., & Holman, G. D. 2010, ApJ, 720, 1472
Brosius, J. W., & Holman, G. D. 2012, A&A, 540, A24
Brosius, J. W., & Phillips, K. J. H. 2004, ApJ, 613, 580
Carmichael, H. 1964, in NASA SP-50, The Physics of Solar Flares, ed. W. N. Hess (Washington, DC: NASA), 451
Chen, F., & Ding, M. D. 2010, ApJ, 724, 640
Culhane, J. L., Harra, L. K., James, A. M., et al. 2007, Sol. Phys., 243, 19
Culhane, J. L., Hiei, E., Doschek, G. A., et al. 1991, Sol. Phys., 136, 89
Del Zanna, G., & Mason, H. E. 2005, A&A, 433, 731
Emslie, A. G., Li, P., & Mariska, J. T. 1992, ApJ, 399, 714
Fisher, G. H., Canfield, R. C., & McClymont, A. N. 1985a, ApJ, 289, 414
Fisher, G. H., Canfield, R. C., & McClymont, A. N. 1985b, ApJ, 289, 425
Fisher, G. H., Canfield, R. C., & McClymont, A. N. 1985c, ApJ, 289, 434
Fletcher, L., Dennis, B. R., Hudson, H. S., et al. 2011, Space Sci. Rev., 159, 19
Fletcher, L., & Hudson, H. S. 2008, ApJ, 675, 1645
Golub, L., Deluca, E., Austin, G., et al. 2007, Sol. Phys., 243, 63
Handy, B. N., Acton, L. W., Kankelborg, C. C., et al. 1999, Sol. Phys., 187, 229
Hara, H., Watanabe, T., Harra, L. K., Culhane, J. L., & Young, P. R. 2011, ApJ, 741, 107
Harra, L. K., Matthews, S. A., & Culhane, J. L. 2001, ApJ, 549, L245
Harrison, R. A., Hood, A. W., & Pike, C. D. 2002, A&A, 392, 319
Harrison, R. A., Sawyer, E. C., Carter, M. K., et al. 1995, Sol. Phys., 162, 233
Hirayama, T. 1974, Sol. Phys., 34, 323
Hurford, G. J., Schmahl, E. J., Schwartz, R. A., et al. 2002, Sol. Phys., 210, 61
Kopp, R. A., & Pneuman, G. W. 1976, Sol. Phys., 50, 85
Kosugi, T., Makishima, K., Murakami, T., et al. 1991, Sol. Phys., 136, 17
Lemen, J. R., Title, A. M., Akin, D. J., et al. 2012, Sol. Phys., 275, 17
Lin, R. P., Dennis, B. R., Hurford, G. J., et al. 2002, Sol. Phys., 210, 3
Smith, D. M., Lin, R. P., Turin, P., et al. 2002, Sol. Phys., 210, 33
Sturrock, P. A. 1968, in IAU Symp. 35, Structure and Development of Solar Active Regions, ed. K. O. Kiepenheuer (Dordrecht: Reidel), 471
Su, Y., van Ballegooijen, A., Lites, B. W., et al. 2009, ApJ, 691, 105
Thompson, W. T. 1999, CDS Software Note 53, http://solar.bnsc.rl.ac.uk/swnotes/cds_swnote_53.pdf
Veronig, A. M., Rybak, J., Gomory, P., et al. 2010, ApJ, 719, 655